

# On-Silicon Neural Activity Monitoring and Time-Frequency Analysis for Early Detection of Epileptic Seizures

Joseph N. Y. Aziz, *Student Member, IEEE*, Rafal Karakiewicz, *Student Member, IEEE*, Roman Genov, *Member, IEEE*, Alan W. L. Chiu, *Member, IEEE*, Berj L. Bardakjian, *Member, IEEE*, Miron Derchansky and Peter L. Carlen

**Abstract**— We present an architecture and very-large-scale integration (VLSI) implementation of a microsystem for neural activity monitoring and time-frequency analysis. The key functional blocks of the microsystem, the integrated neural interface and the wavelet transform processor, have been prototyped in a 0.35- $\mu\text{m}$  standard complementary metal-oxide-semiconductor (CMOS) technology. Its utility is validated in autonomous early detection of epileptic seizures in an *in vitro* epilepsy model of recurrent spontaneous seizures in mouse hippocampal brain slices.

**Index Terms**— Epilepsy, Seizure detection, Seizure prediction, Integrated neural interface, Wavelet transform.

## I. INTRODUCTION

APPROXIMATELY 50 million people worldwide are epileptic. While epilepsy is the third most common neurological disorder following stroke and Alzheimer's disease, it carries higher cost to the society than stroke. Present day therapy to control epilepsy includes several strategies with various degrees of efficacy.

Pharmacotherapy requires the long-term use of systemically administered drugs, which in some cases are toxic [1]. Surgery involves the excision of a relatively large volume of brain tissue, with the concern of neurological disability

This work was supported by Natural Sciences and Engineering Research Council of Canada (NSERC) and Krembil Fund.

J. N. Y. Aziz was with the Department of Electrical and Computer Engineering, University of Toronto, Toronto, ON M5S 3G4, Canada. He is now with Broadcom Corporation, Singapore, 757716 (email: joseph@eecg.utoronto.ca).

R. Karakiewicz was with the Department of Electrical and Computer Engineering, University of Toronto, Toronto, ON M5S 3G4, Canada. He is now with SNOWBUSH Microelectronics, Toronto, ON M5G 1Y8, Canada (e-mail: raf@snowbush.com).

R. Genov is with the Department of Electrical and Computer Engineering, University of Toronto, Toronto, ON M5S 3G4, Canada (email: roman@eecg.utoronto.ca).

A. W. L. Chiu is with the Department of Biomedical Engineering, Louisiana Tech University, Ruston, LA 71272, USA (email: alanchiu@latech.edu).

B. L. Bardakjian is with the Institute of Biomaterials and Biomedical Engineering, Department of Electrical and Computer Engineering, University of Toronto, Toronto, ON M5S 3G9, Canada (e-mail: berj@cbl.utoronto.ca).

M. Derchansky, and P. L. Carlen are with the Toronto Western Research Institute and the Department of Physiology, University of Toronto, Toronto, Canada (e-mail: carlen@uhnres.utoronto.ca).

from the removal of either normal or functionally necessary tissue. Also there is the real but small risk of any invasive neurosurgical operation.

Approximately 60 percent of epileptic patients suffer partial seizures, 30 percent of whom are intractable and do not respond to medication. A significant percentage of these patients are not suitable for surgical therapy. For such patients, brain stimulation is presently done via peripheral nerve stimulation (*i.e.*, vagal) or via implanted electrodes using protocols which are often empiric, and have no direct relationship to the underlying neuronal dysfunctional activity [2], [3], [4]. Continuous vagal nerve stimulation is often effective in reducing the number of seizures in patients with intractable epilepsy, but only five percent of treated patients have been rendered seizure-free [2]. Deep brain stimulation of the thalamus and white matter has recently been discussed [3], [4]. Several studies have used continuous open-loop electrical stimulation [5], [6], [7]. These and many other results are significant and suggest that efficacy of open-loop methods for seizure control can be further improved by feedback techniques.

The evolution of a seizure involves a preictal (*i.e.*, prior to seizure) transitional state that dynamically differs from the interictal (*i.e.*, between seizures) and ictal (*i.e.*, during seizure) states [8]. We define the onset of a preictal activity as that when the complexity (as measured by the maximum Lyapunov exponent) of the higher frequency (super gamma) activity begins to decrease, whereas the ictal activity is defined as that when the complexity of the higher frequency activity is at its minimum value. Clinically, when recording intracranially or extracranially, there are often clear electrographic changes which can be seen before the clinical seizure starts, although the opposite also often occurs wherein the clinical seizure manifests prior to clearcut electrographic abnormalities. This is presumed to be in part due to the position of the recording electrodes, be it near or far from the site of seizure activity and onset.

The implication of this distinction in the states is that there is a possibility for seizure detection or prediction and subsequent preventive intervention. Previous studies have reported algorithms which detect the ictal state and stimu-

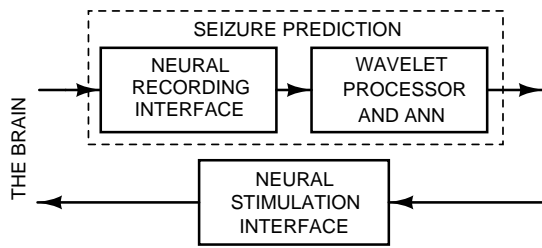


Fig. 1. The top-level block diagram of an implantable medical device for autonomous prediction and prevention of seizures. The device is implemented as a dynamic control loop that consists of feedforward and feedback pathways to predict and prevent intractable seizures respectively.

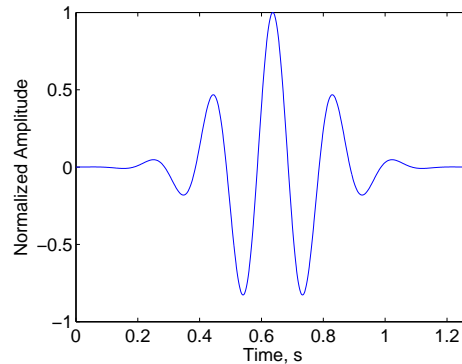


Fig. 2. A Morlet wavelet with a 5Hz center frequency.

late to stop it, often leading to reduction in the number of seizures [9] with as many as 17 percent of treated patients rendered seizure-free [10]. These important results suggest that early detection of the preictal state before the clinical seizure manifests itself may further enhance the efficacy of automated seizure control. Although preictal states are not always apparent on the human electroencephalogram (EEG), they usually are very clearly apparent (exhibit themselves well) in *in vitro* and *in vivo* animal seizure models. This work employs an *in vitro* epilepsy model of recurrent spontaneous seizures in mouse hippocampal brain slices [11]. Thus in the remainder of this work we refer to our early seizure detection strategy as seizure prediction as valid in animal models.

Control of seizures by electrical stimulation can be considered as control of a dynamical system with the goal of keeping it away from the stable manifold. Once the stable manifold is firmly established, this becomes a laborious and challenging task. Consequently, in this context, the ultimate prerequisite for any control algorithm is the ability to predict the onset of undesirable dynamics prospectively, not to detect it retrospectively. Hence, the real-time prediction of state transitions becomes the key to a successful control strategy.

A number of effective methods have been developed to find the earliest possible cues to an epileptic seizure onset. They include power spectrum, principal component analysis, phase correlations, correlation dimension, Lyapunov exponents and wavelet artificial neural networks [12], [13], [14], [15], [16]. A thorough review of seizure prediction algorithms can be found in [17]. The seizure prediction method utilizing wavelet artificial neural networks (WANNs) is chosen in this work for its suitability for an implantable hardware implementation. The inherently parallel architecture of a WANN can be directly mapped onto a compact low-power silicon microchip. Additionally, WANNs perform well in presence of differences among subjects, and do not require parameter adjustment or any assumptions about biological signals which are often highly non-stationary.

In this paper we present the design and experimental validation of key functional blocks of an implantable device that senses, amplifies, adaptively learns and clas-

sifies the abnormal brain activity of epilepsy in order to predict seizures before they take place. Figure 1 depicts a simplified block diagram of the envisioned autonomous seizure prediction microsystem with a preventive feedback shown. The feedforward signal path predicts a seizure. The feedback path activates a therapeutic intervention upon a positive prediction. The intervention can be in the form of an electrical stimulation [18], [19], or a chemical anticonvulsant injection [20]. In this paper we focus on a miniature implantable implementation of the key components of the feedforward seizure-predicting path.

The rest of the paper is organized as follows. Section II introduces the WANN seizure prediction algorithm. Section III presents a VLSI implementation of the main functional blocks of the microsystem for seizure prediction. Section IV contains the experimental results validating the functionality and efficacy of the microsystem.

## II. SEIZURE PREDICTION ALGORITHM

It has been demonstrated in many instances that frequency domain information was important for seizure or seizure-like event (SLE) onset prediction [21], [22], [23], [24]. Significant changes in power spectra of various frequency bands had been found within 20-second time windows preceding transitions to SLEs in rats [25], [26]. It was also observed that as the extracellular electrical field recording moved from an interictal state towards a preictal state, higher frequency components appeared with progressively greater energies. Using sensitivity measures and principles of set theory, it was demonstrated that delta (<4Hz), super gamma (100-250Hz) and fast ripple (250-400Hz) frequency bands are critical for accurate classification [27]. This observation suggested the importance of high frequencies (*i.e.*, above 100Hz) during the development of SLEs and that the time-frequency information can serve as a significant precursor to an epileptic seizure. Frequency-related information may be related to the entrainment of neuronal population firing. High-frequency epileptiform oscillation is suggested to be useful in localizing regions of seizure onsets and in understanding the mechanisms behind seizure generation.

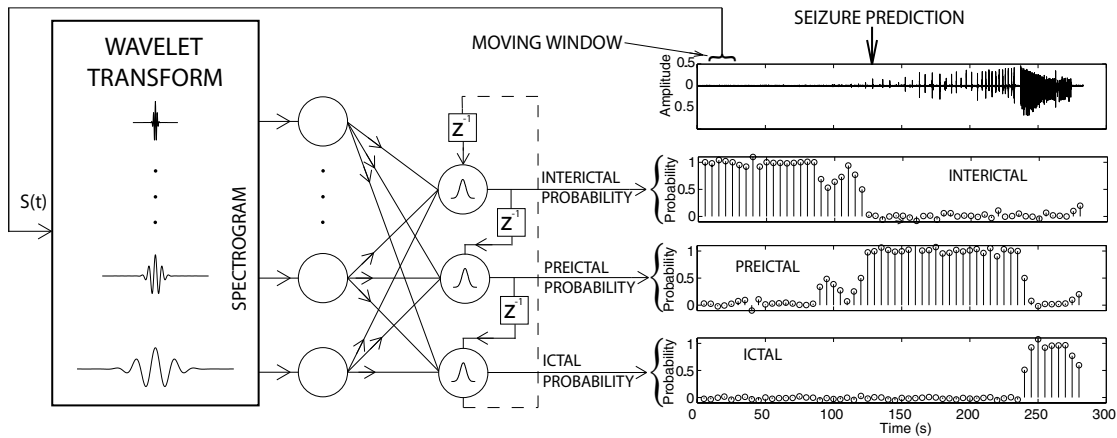


Fig. 3. Architecture of the WANN (two layers of the neural network are shown for simplicity). Each WANN output unit generates an estimate between zero and one, at fixed time intervals, denoting the probability of one possible system state (interictal, preictal or ictal). An example of a seizure recording in the seizure data set and resulting WANN outputs is shown.

Wavelet transforms are commonly used to generate a signal spectrum that is localized in time. They have been employed for spike and seizure localization [28] and to determine the start times of seizures [29], both in multi-channel subdural EEG data. Wavelet transforms combined with artificial neural networks (ANNs) are well suited for predicting seizures because ANNs can learn to generalize and solve complex problems, while wavelet transforms can generate time-varying frequency domain features [16], [23]. These WANNs are suitable for processing biological signals because of their inherent nonlinearity. The utilization of time-varying frequency information as the input feature for state classification was the direct result of experimental findings reported in [21] and [24]. A major advantage of a WANN is that it captures variations in the recorded extracellular field potentials during the progression of SLE episodes. The intrinsic characteristics of the WANN training allow easy elimination of the “common” frequency information. Therefore, WANN is a connectionist approach to understanding the relationship between the variation of the frequency over time and the current seizure state.

The WANN was initially implemented in software in order to validate its functionality. Morlet wavelets are employed [30]. The Morlet wavelet is a locally periodic wavetrain constructed by localizing a complex sine wave with a Gaussian envelope [31] as shown in the example in Figure 2. Appropriate frequency bands in the range of 0-400Hz are selected as input sequences to the ANN [27]. The WANN utilizes the time-frequency distribution of the recorded biological signals as its input layer and generates the probability of seizure states at its output. The synaptic weights of the WANN were trained using back-propagation supervised learning [32].

Training and testing of the WANNs was done on *in vitro* extracellular field recordings from rat hippocampal slices. The training set includes data from 14 rats containing a total of 50 seizure episodes. The test set consists of *in vitro*

extracellular field recordings from the same rats containing 52 seizure episodes. Neural signals were recorded with a commercially available bench-top instrumentation amplifier at 1kHz sampling rate. Hippocampal slice recordings were obtained from male Wistar rats (17-25 days old). Spontaneous recurrent seizure events were induced by superfusing the slice with an artificial cerebrospinal fluid (ACSF) solution containing 0.5mM  $Mg^{2+}$  [33], [11]. This seizure model has a characteristically short preictal phase. The duration of preictal activities in the data set ranged between 15 seconds and 120 seconds.

The wavelet transform was computed over overlapping moving time windows of 9.5 seconds that capture the time-frequency content of the recorded neural data at 2 second intervals (*i.e.*, there is a 7.5 second overlap between successive time windows). Based on the data, the optimum network consists of 40 input units representing the power of the appropriate frequency bands, a hidden layer of size 100 and the output layer of size four. Each output node represents one of the possible states (interictal, preictal, ictal, and none of the above).

Figure 3 depicts the architecture of the WANN and includes an example of how the WANN classified data from a recorded test data set. An episode from a test data set with an *in vitro* extracellular field recording over approximately 280 seconds containing one SLE is shown. A corresponding time-frequency map was computed using Morlet wavelets with 40 frequency bins ranging between 0Hz and 400Hz. In this example, an ictal state onset was identified at  $t=240s$  as shown at the bottom right of Figure 3. The WANN was able to successfully and accurately recognize preictal activity as early as 120 seconds prior to the ictal onset by choosing the output with the highest probability. When tested on the test set, the WANN predicted 90 percent of SLEs as early as preictal states started with approximately 15 percent of false predictions. We have also performed preliminary experiments with human data, confirming the utility of the WANN in early

seizure detection *in vivo*. Results of these experiments once completed will be reported elsewhere.

A number of other wavelet-based strategies for classification of ictal activities have been reported [34], [35], [36], [37], [38], [39]. Daubechies level-four wavelet transform formulated as a 22-coefficient finite impulse response filter is employed in [34] and [35]. This algorithm involves selection of filter characteristics appropriate for a recorded signal. In our approach, the neural network pruning strategy selects appropriate combination of frequency band features in an automated manner. The topology of the network is also tunable based on standard pruning techniques. Furthermore, the ANN allows for the estimation of nonlinear relations between the different frequency component and the observed pathological states of the brain. In [36] the importance of selecting suitable mother wavelet and using multiple features such as energy, variance and relative amplitude for classification is addressed. This may require certain subjectivity, such as in setting appropriate thresholds. In our case, the threshold of the output units of the ANN is selected based on the curvature of the receiver operating characteristic (ROC) obtained on the validation data set. In [37] wavelets are utilized to isolate frequency subbands, before complexity and chaoticity are measured. Both of these measures may require some degree of subjectivity in choosing the linear regions. Compared to [38] and [39] our network uses a wider range of frequency and subsequently prunes out irrelevant frequency bins.

### III. VLSI IMPLEMENTATION

The neural activity monitoring and time-frequency analysis microsystem implements the main components of the WANN seizure prediction algorithm described above on a miniature low-power platform. It forms the feedforward path of the block diagram in Figure 1 consisting of the neural recording interface and the wavelet processor with an ANN.

The envisioned implantability limits the size of the microsystem to under one square centimeter. Additionally, the amount of power dissipated by the microsystem is limited by tissue heating constraints. Preliminary reports suggest that heat dissipation resulting in heating of the cortex tissue by one degree Celsius is safe, which corresponds to power density of approximately  $80\text{mW}/\text{cm}^2$  [40]. This section presents validation of feasibility of a compact and low-power VLSI implementation of the neural recording interface and the wavelet processor, with the ANN implemented in software.

#### A. Neural Recording Interface

Most of the frequency content of the extracellular neural activity in the brain is concentrated below 5 kHz. Neural signals amplitude typically ranges from a few microvolts to a few millivolts. The primary function of the neural

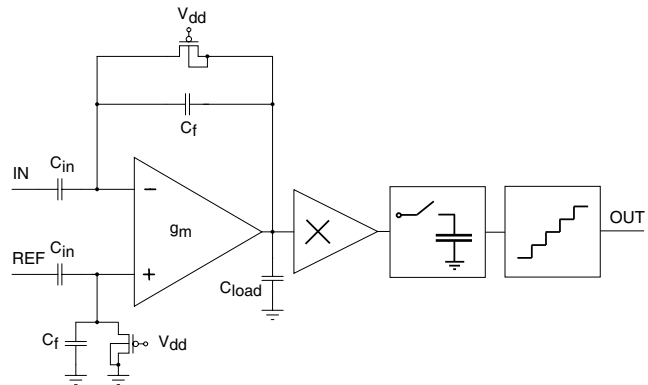


Fig. 4. Architecture of the neural recording interface comprised of the neural pre-amplifier and band-pass filter, the second-stage programmable-gain amplifier, the sample-and-hold cell, and the A/D converter.

recording interface is to amplify such weak neural signals with minimal circuit noise and non-linearities added to the output. Due to electro-chemical effects at the tissue-electrode interface, DC voltage offsets with several orders of magnitude above the actual signal level are common across differential recording electrodes and have to be removed.

The main functional components of the neural recording interface are shown in Figure 4. The neural signal is filtered, amplified and digitized. The channel employs two stages of amplification with the first stage including a band-pass filter, and the second stage having a programmable gain. The high-pass filter (HPF) blocks the random DC voltage offset at the tissue-electrode interface in order to avoid amplifier saturation. The low-pass filter (LPF) limits the effect of out-of-band noise and acts as an anti-aliasing filter. The subsequent sample-and-hold circuit samples the analog voltage and holds it on a capacitor as needed for the analog-to-digital converter (ADC).

The tolerable internal circuit noise level of the channel dictates the minimum amount of power consumption per channel and minimum dimensions of each channel. A critical component of the neural recording interface is the first-stage amplifier as it dominates the noise, power and area requirements. The amplifier in the first stage of the channel is a wide-swing transconductance amplifier with the current-mirror topology optimized for low-noise operation under power and area constraints [41]. In the closed loop configuration, the overall midband gain of the amplifier is determined by the ratio of the capacitors  $\frac{C_{in}}{C_f}$ . Based on thermal noise considerations,  $C_{in}$  is chosen to be 5pF. The 100fF feedback capacitor  $C_f$  yields the mid-band gain of 50. The low-pass corner frequency is determined by the first stage and is approximately equal to  $\frac{g_m}{2\pi C_{load}} \frac{C_f}{C_{in}}$ . It is tunable in the range of 1kHz to 10kHz as controlled by the bias current of the differential input stage. The high-pass corner frequency is  $(2\pi C_f R_f)^{-1}$ , where  $R_f$  is the resistance connected in parallel with  $C_f$ . To achieve a HPF cut-off frequency below 0.1Hz, a large

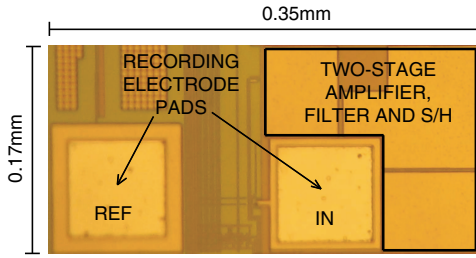


Fig. 5. Micrograph of the main components of the integrated neural interface fabricated in a  $0.35\text{-}\mu\text{m}$  CMOS technology.

resistance is implemented as a MOS device biased in the subthreshold region of operation [42]. As preserving local field potentials is important in seizure prediction, the gate of the high-resistance pMOS transistors is connected to Vdd. In general, the HPF cut-off frequency can be tuned by varying this voltage.

The noise requirements of the second stage are reduced by the gain of the first stage. The second stage employs the same amplifier topology as the first stage, but can be biased at a lower power. Gain programmability is achieved by a configurable bank of capacitors in the feedback of the second stage. The gain ranges between 200 and 5000, with the output voltage range of 1.5V.

The sample-and-hold circuit employs a capacitor with input-independent charge injection, buffered by a source follower. The ADC utilizes an algorithmic switched-capacitor topology with four-phase clocking insensitive to capacitor mismatch [43]. The ADC resolution of 8 bits is sufficient for epileptic seizure prediction as described here and can be extended at the expense of moderate increases in power dissipation and integration area if needed in other applications.

A micrograph of the neural recording interface fabricated in a  $0.35\text{-}\mu\text{m}$  CMOS technology is shown in Figure 5. The experimentally measured amplifier input-referred noise is  $13\mu V_{rms}$  over the 10Hz-10kHz bandwidth. This corresponds to less than 0.7LSB at 5mV input voltage range and 8-bit ADC resolution. The two-stage neural amplifier, filter and sample-and-hold circuit occupy approximately  $0.03\text{mm}^2$  area. The two-stage neural amplifier and filter dissipate  $23\mu\text{W}$  of power. The sample-and-hold circuit dissipates  $33\mu\text{W}$  at the sampling rate of 10ksps. The ADC occupies  $0.025\text{mm}^2$  area and dissipates  $327\mu\text{W}$  of power at 50ksps sampling rate as measured on a separate test chip. The results are comparable to characteristics of other previously reported integrated neural interfaces [41], [44], [45], [46], [47].

The power dissipation and integration area characteristics of the neural interface allow for its multi-channel implementations on a single chip. Simultaneous recordings on hundreds of sites in the brain can be performed [48]. Multi-site recordings yield spatial information about a seizure such as its foci and spatial progression [49]. Such multi-channel neural interface implementations yield a

vast amount of data [50], [51]. Due to the prohibitive computational complexity, these data generally have to be reduced before an on-chip seizure prediction algorithm can be applied. Multi-channel spike detection has been employed for neural data reduction [52] but may be of limited use for seizure prediction. Another approach is to perform on-chip temporal differentiation of recorded signals [53] in order to identify an optimal recording site where the WANN algorithm is to be invoked. Other seizure localization methods based on multi-channel EEG recordings have been reported [28]. Currently, on-chip seizure detection and prediction in multi-site intracranial neural recordings remain a subject of extensive research.

### B. Wavelet Processor

The WANN seizure prediction algorithm described in Section II requires extensive computing resources to compute the wavelet transform and to perform weight multiplication in the two layers of the ANN. The computational core of these linear transforms can be expressed in terms of vector-matrix multiplication (VMM) which implies calculation of products between input vectors and a pre-determined matrix of coefficients. The required computational throughput is beyond the capabilities of conventional digital processors, particularly given a small power budget, as they are typically limited by the serial nature of their architectures and low memory bandwidth. Due to its inherent parallelism, VMM lends itself well to high-throughput parallel computing architectures. The parallel architecture of the WANN implementation presented here is depicted in Figure 6 (left). Each linear transform is computed on a corresponding computing array.

The discrete wavelet transform is computed by correlating the input with a set of precomputed wavelets of different frequencies stored on an array. Instead of a conventional tree-based approach, wavelet coefficients are computed in parallel. The frequencies of wavelets dictate the dimensions of the array. As shown in Figure 2, most of the energy of the Morlet wavelet falls within an interval equal to five periods of the wavelet. For the lowest Morlet wavelet frequency of 5Hz and the sampling rate of 1ksps, an array with 1024 input dimensions is needed (*i.e.*,  $N=1024$ ). The highest Morlet wavelet frequency is 400Hz. To accommodate 40 frequency bins in this range, the array has 40 outputs (*i.e.*,  $M=40$ ). A correlation of the input vector with the set of wavelets is computed for every sample, every 1ms. The outputs of the array are accumulated by the accumulator over the duration of the input moving window. The accumulator performs one addition per millisecond and is of low computational complexity.

As the wavelet matrix is large, an analog VLSI implementation of the parallel computational array of the wavelet processor is desirable as it can yield high integration density [54]. In addition to high integration density analog VLSI implementations can achieve high energy

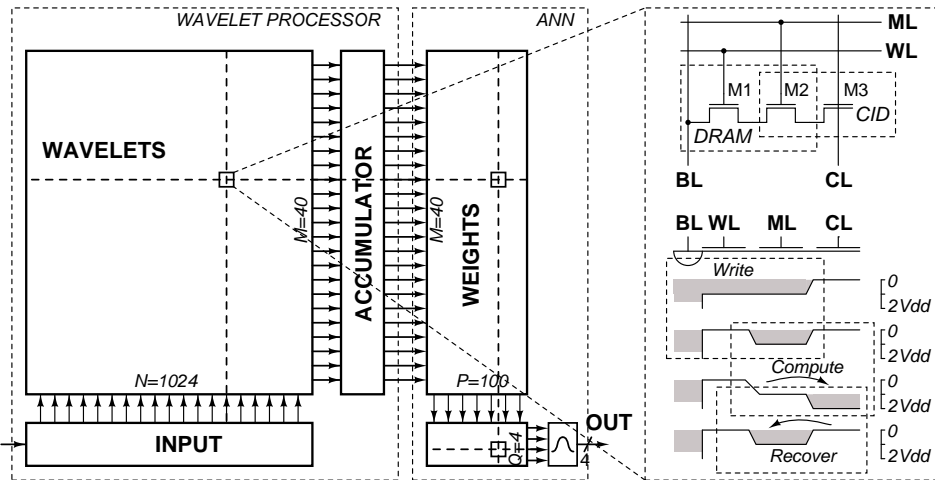


Fig. 6. Parallel WANN architecture (left), circuit diagram of CID computational cell with integrated DRAM storage (right, top), and charge transfer diagram for active write and compute operations (right, bottom).

efficiency [55], [56]. These benefits may come at the cost of reduced accuracy [54], [56], which is often not critical in neural recording applications.

We designed, prototyped and experimentally validated a massively parallel mixed-signal (*i.e.*, analog-digital) VLSI processor for computing linear transforms such as Morlet wavelet transform. Internally analog, externally digital VMM computation combines the energy efficiency and density of analog array processing with the precision of digital processing, and the convenience of a programmable and reconfigurable digital interface.

Each unit cell in the wavelet processor array shown in Figure 6 (right) is comprised of a dynamic random access memory (DRAM) cell and a charge-injection device (CID) [57] cell, both sharing transistor M2. During the *write* operation the data to be stored is broadcast on the vertical bit-lines (BLs), which extend across the array. A row to be written to is selected by activating its word-line (WL) turning transistor M1 on. The output match-line (ML) is held at  $V_{dd}$  during the *write* phase creating a potential well under the gate of transistor M2. This potential well is filled with electrons or emptied depending on whether the BL is logic-one or logic-zero respectively. Logic-one on BLs corresponds to 0V, while logic-zero corresponds to  $V_{dd}$ . During the *compute* operation, the input data is broadcast on the compute-lines (CLs) while MLs, previously precharged to  $V_{dd}$ , are now left floating. Logic-one CL bit corresponds to voltage  $2V_{dd}$ , while logic-zero corresponds to 0V. Each cell performs a one-quadrant binary-binary multiplication between its stored logic value and its CL logic value. An active charge transfer from M2 to M3 can occur only if there is a non-zero charge stored, and if the potential on the gate of M3 rises above that of M2, to  $2V_{dd}$ . In this case, the high-impedance gate of M2 couples to its channel and raises above  $V_{dd}$  by a fixed voltage depending on the charge and capacitance of M2. The cell performs non-destructive computation since the

transferred charge is sensed capacitively on the MLs. Once computation is performed, the charge is shifted back from M3 into the DRAM storage transistor M2.

Capacitive coupling of all cells in a single row into a single ML implements zero-latency analog accumulation along each row. An array of cells thus performs analog multiplication of a binary vector with a binary matrix. The analog array is interfaced with a bank of on-chip row-parallel ADCs to provide convenient digital outputs. The architecture is scalable, limited only by sensitivity of sense amplifiers and accuracy of row-parallel analog addition. It easily extends to multi-bit data with wavelets stored in a bit-parallel form in the array (*i.e.*, an  $I$ -bit wavelet is stored on  $I$  rows of the array) and inputs presented bit serially (a  $J$ -bit input takes  $J$  clock cycles to be fed in) [58].

An integrated prototype of the wavelet processor fabricated in a  $0.35\mu\text{m}$  CMOS technology is shown in Figure 7. Morlet wavelet templates are stored in the four on-chip  $128 \times 256$ -cell DRAM-based analog arrays in a row-parallel fashion. The arrays are configured in a  $128 \times 1024$  organization (*i.e.*,  $1 \times 4$  arrays) to accommodate low-frequency wavelets as discussed earlier. Input data are presented serially into the input shift registers of the four arrays. In every computational cycle, a 1024-sample window of the input signal is correlated with 32 4-bit wavelet templates stored in the on-chip memory in a bit-parallel format. The wavelet frequency ranges from 5Hz to 300Hz. Correlation is performed in parallel on each array, in 256-sample segments per array. The computed partial inner products are quantized by four banks of 128 row-parallel ADCs and added in digital domain to yield full 1024-component inner products. The processor prototype performs  $128 \times 1024$  binary multiplications and analog accumulations for every input sample. At 13.7kHz computing frequency, the four-quadrant array delivers 1.8 billion binary multiply-and-accumulate operations per second and dissipates  $95\mu\text{W}$  of power, which corresponds to computational efficiency

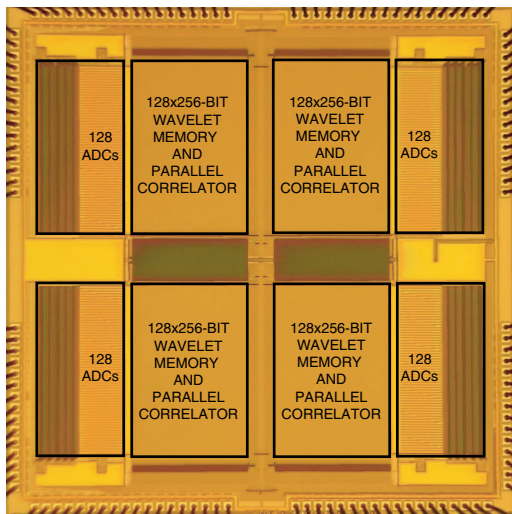


Fig. 7. The wavelet processor prototype micrograph and floorplan. The die was fabricated in a  $0.35\text{-}\mu\text{m}$  CMOS technology and occupies an area of  $4\text{mm} \times 4\text{mm}$ .

of over 19 billion binary operations per second for every milliwatt of power. A further 25-fold improvement in energy efficiency can be achieved by adiabatic clocking, with the total load capacitance of the array resonating with an off-chip inductor in order to generate a sinusoidal waveform clock [59].

Not included in the power dissipation figure are the power dissipated in the ADCs and other peripheral circuits such as control logic, shift registers and sense amplifiers. The bank of 512 ADCs dissipates  $6.3\text{mW}$  at  $15\text{ksp}$ s sampling rate. When the ANN is implemented in the analog VLSI domain the ADCs are not needed, but are included in the current implementation for convenience and flexibility of testing. Other peripheral digital circuits are operated at kHz clock speeds which ensures their low power dissipation.

The seizure prediction algorithm described in Section II utilizes 40 frequency bins with 8-bit encoded wavelet coefficients. This is beyond the capacity of the fabricated processor due to the costs of low-volume prototyping. To accommodate these requirements the small-scale prototype in Figure 7 has to be scaled up by a factor of 2.5 in the number of rows (320 rows instead of existing 128, to store 40 8-bit wavelets instead of 32 4-bit wavelets). This can be easily accomplished by increasing the number of rows in each one-quadrant array to 160 and doubling the number of arrays, for a total chip area of under  $40\text{mm}^2$  and a proportional increase in power dissipation.

### C. ANN

The ANN classifies the underlying dynamics of spontaneous *in vitro* events into interictal, preictal and ictal neural activity based on the Morlet wavelet features of the neural signal computed on the wavelet processor. The number of hidden nodes of the ANN,  $P$ , is 100, and the number of

the output nodes,  $Q$ , is 4 as shown in Figure 6 (left). It performs one classification per input moving window, every 2 seconds. The computational complexity of the ANN is four orders of magnitude less than that of the wavelet transform (one order in matrix dimensions and three orders in time).

As the computational requirements and integration area of the ANN are negligibly small compared to those of the wavelet transform, it can be easily synthesized in digital VLSI domain, with relatively small integration area and power dissipation. Mixed-signal and analog VLSI implementations are also feasible. In fact, one simple way to implement the ANN is to re-use the same design as that employed for the wavelet processor. An example of such an implementation of a neural network is given in [60]. To multiply 40 inputs by 100 8-bit weights each, a  $800 \times 40$  array of CID/DRAM cells is sufficient. Multiplying 100 hidden nodes by four weights each and computing four non-linear functions on the output nodes requires small additional resources. Further reduction in power dissipation of the system can be obtained by eliminating the ADC bank in the wavelet transform processor and by employing a fully analog ANN implementation such as the one reported in [61]. This comes at the cost of reduced programmability and possibly limited accuracy.

As the ANN can be implemented by re-using the same computing technology and requires negligibly small computing resources and thus small integration area and power, its prototyping is not needed to validate the feasibility of such a VLSI implementation. To maintain the flexibility needed in experimental training and run-time operation of the prototype, in this work the ANN was implemented in software.

## IV. EXPERIMENTAL VALIDATION

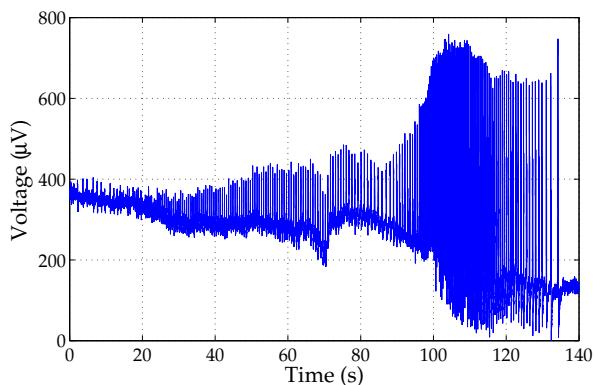
Both the functionality of all main components of the microsystem, and its efficacy in seizure prediction have been experimentally validated as described next.

### A. Functionality Validation

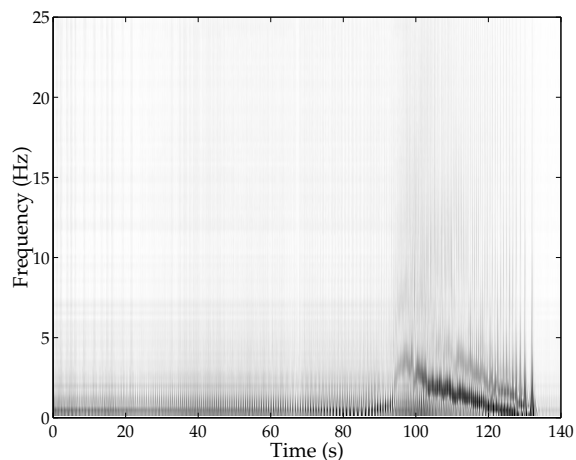
In order to validate the functionality of the microsystem, the two main components, the neural recording interface and the wavelet processor described in the previous section, were experimentally characterized in seizure recording and time-frequency analysis.

The functionality of the neural recording interface has been validated in *in vitro* extracellular neural activity recording experiments. The recording channel was connected to differential recording electrodes. The electrodes were inserted in a rat hippocampus where SLEs were induced in the presence of low  $Mg^{2+}$  ACSF [11]. Figure 8(a) shows a SLE recording *in vitro* from a rat hippocampus amplified and filtered by the neural recording interface chip.

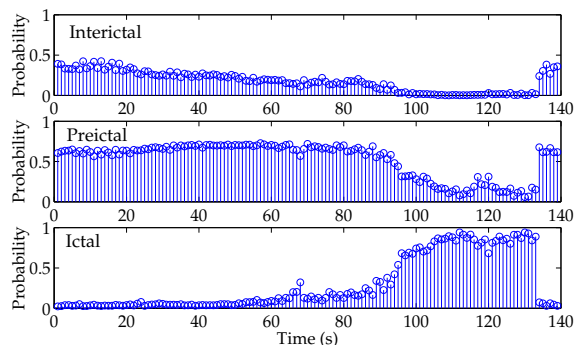
The neural recording in Figure 8(a) was fed to the input of the wavelet processor. To validate the functionality of



(a)



(b)



(c)

Fig. 8. (a): An example of a seizure recording performed by the neural recording interface chip; (b): a corresponding time-frequency map computed on the wavelet transform processor chip; and (c): resulting ANN outputs. Each output unit generates an estimate between zero and one, at fixed time intervals, denoting the probability of one possible system state (interictal, preictal or ictal).

the wavelet processor, a time-frequency map of this recording was computed on-chip. The output of the processor represents the time-frequency map of the acquired signal. Figure 8(b) depicts the time-frequency map of the SLE recording shown in Figure 8(a) computed by the wavelet processor. The frequency range from 0.6Hz to 25Hz with the recording downsampled by a factor of 10 was chosen in this experiment in order to visually validate the accuracy of the time-frequency map. Below 5Hz at the start of the ictal state, seizures have two characteristic energy bands with their frequencies linearly decreasing over time. These bands can be clearly observed on the time-frequency map in Figure 8(b). A software emulation of the processor in Matlab yields identical results.

The time-frequency map computed and quantized on the wavelet processor was fed into the software-based ANN. Figure 8(c) shows the outputs of the ANN classifying the recording in Figure 8(a) using the time-frequency map in Figure 8(b) as its input. In this example, the network detects the onset of the preictal and ictal states adequately even in the absence of high-frequency information. As described in the next section, high-frequency Morlet wavelet coefficients were computed on the wavelet processor in order to validate its efficacy in seizure prediction.

### B. Efficacy Validation

The efficacy of the neural activity monitoring and time-frequency analysis microsystem in predicting seizures was validated on an *in vitro* extracellular field recording data set. As detailed in Section II, the low- $Mg^{2+}$  *in vitro* model of spontaneous recurrent seizure in mouse hippocampal slices was utilized. The training and test sets include data from 14 rats containing a total of 102 seizure episodes sampled at 1kHz.

Time-frequency maps of *in vitro* extracellular field recordings in this data set were computed on the wavelet processor shown in Figure 7. Time-frequency maps of time windows corresponding to 50 seizure episodes were used to train the ANN. The ANN was tested on time windows corresponding to the remaining 52 seizure episodes. The microsystem correctly detects 90 percent of seizures with 50 percent false positive rate. These results are identical to those obtained by emulating the hardware in Matlab.

The high false positive rate is due to simplifications in the prediction algorithm made in order to reduce the integration area of its on-silicon implementation (32 frequency bins from 5Hz to 300Hz at 4-bit resolution). When the wavelet processor capacity is extended to include 40 frequency bins at 8-bit resolution ranging from 5Hz to 400Hz, it is expected that approximately 90 percent of seizures will be predicted correctly with approximately 15 percent of false predictions, as detailed in Section II.

To reduce the false positive rate in the hardware-based implementation, the recorded neural activity episodes classified as seizures by the microsystem are subsequently fed to the WANN seizure prediction algorithm trained on the

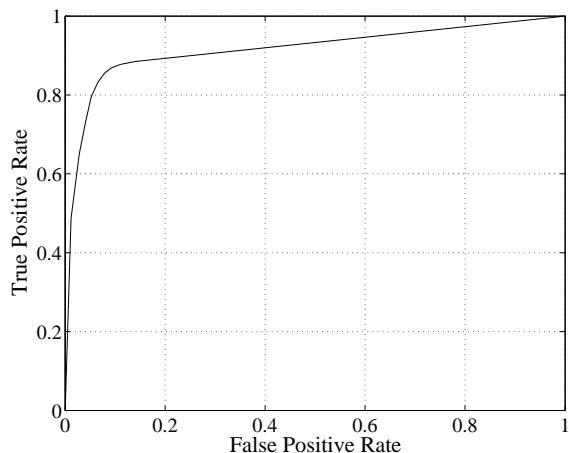


Fig. 9. Receiver operating characteristic (ROC) of the system.

same data set. The software-based classification is only triggered whenever the hardware makes a positive prediction. As the number of non-seizure episodes is usually much greater than the number of seizure episodes, this double-pass approach yields savings in the computational load of a factor of two which makes the WANN algorithm suitable for implementing on a low-power digital signal processor (DSP).

The resulting relationship between the true positive rate and the false positive rate in seizure prediction is described by the ROC curve shown in Figure 9. The depicted ROC demonstrates that approximately 85 percent of seizures in the test data set were predicted correctly as soon as a preictal state started with approximately 8 percent of false predictions. According to Figure 1, this translates into an 8 percent overhead in therapeutic brain stimulation. This is a significant improvement in selectivity of brain stimulation compared to currently available continuous stimulation techniques [2].

### C. Area and Power Considerations

As described in Section III, the area of the large-scale implementation of the seizure prediction microsystem accommodating 40 frequency bins with 8-bit coefficients is dominated by the array computing the wavelet transform. The wavelet transform processor is estimated to occupy over 90 percent of the silicon area, with the remaining 10 percent utilized by the integrated neural interface and an on-chip implementation of the ANN. The total silicon area is estimated to be under  $45mm^2$ . Such a die size is well within maximum die size limitations of the VLSI technology as dictated by yield considerations.

Given the area of the microsystem, the power density of  $80mW/cm^2$  deemed safe for the cortex [40] yields the total power budget of  $36mW$ . As detailed in Section III, the total power dissipation of the large-scale implementation of the seizure prediction microsystem is well within this budget, ensuring heat dissipation that is safe for the brain tissue.

TABLE I  
SUMMARY OF SYSTEM CHARACTERISTICS

<b>NEURAL INTERFACE</b>	
Programmable Gain	46dB - 74dB
Input-referred Noise	$13\mu V_{rms}$
Noise Bandwidth	10Hz - 10kHz
LPF Cut-off Frequency	1kHz - 10kHz
HPF Cut-off Frequency	below 0.1Hz
Max Sampling Rate	40ksps
Integration Area	$0.055mm^2$
Power Dissipation	
Amplifier	$23\mu W$
S/H circuit, 10ksps	$33\mu W$
ADC, 50ksps	$327\mu W$
<b>WAVELET PROCESSOR</b>	
Wavelet Coefficient Resolution	4-bits
Memory Dimensions	$128 \times 1024$
Wavelet Frequency Range	5Hz - 300Hz
Number of Frequency Bins	32 bins
Integration Area	$16mm^2$
Power Dissipation	
Array, 13.7kHz	$95\mu W$
ADC bank, 15ksps	$6.3mW$

This makes the system suitable for early seizure detection *in vivo*. While initial *in vivo* experiments can be performed on animals with implanted recording electrodes connected to the system by an electro-magnetically shielded cable, full implantation will require adding auxiliary circuits such as biasing network and clock generation circuits as well as a wired or wireless communication interface.

A summary of experimental characteristics of the system is given in Table I.

## V. CONCLUSION

We have presented an architecture and VLSI implementation of a neural activity monitoring and time-frequency analysis microsystem for early detection of epileptic seizures. The microsystem is comprised of a neural recording interface for acquiring extracellular neural activity, and a wavelet ANN processor for real-time time-frequency analysis and anticipating the onset of a seizure. The neural recording interface and the wavelet transform processor have been prototyped in a  $0.35\text{-}\mu m$  CMOS integrated circuit technology. The main components of the microsystem were experimentally validated in recording electrical activity of the rat brain and its time-frequency analysis. Performance of the silicon prototype validates the effectiveness of the approach in early detection of epileptic seizures.

## ACKNOWLEDGMENT

The authors thank the Canadian Microelectronics Corporation (CMC) for providing fabrication services.

## REFERENCES

- [1] W. R. Garnett, "Epilepsy," in *Pharmacotherapy: A Pathophysiologic Approach, 3rd ed.*, Dipiro JT, Talbert RL, Yee GC, Matzke GR, Wells BG, Posey LM, eds. Appleton and Lange, Stamford, CT, 1997, pp. 1179–1209.
- [2] E. Ben-Menachem, "Vagus-nerve stimulation for the treatment of epilepsy," *The Lancet Neurology*, vol. 1, no. 8, pp. 477–482, November 2002.
- [3] M. Hodaie, R. Wennberg, J. Dostrovsky, and A. Lozano, "Chronic anterior thalamus stimulation for intractable epilepsy," *Epilepsia*, vol. 43, no. 6, pp. 603–608, June 2002.
- [4] A. A. Cohen-Gadol, M. R. Stoffman, and D. D. Spencer, "Emerging surgical and radiotherapeutic techniques for treating epilepsy," *Current Opinion in Neurology*, vol. 16, no. 2, pp. 213–219, April 2003.
- [5] R. P. Lesser, S. H. Kim, L. Beyderman, D. L. Miglioretti, W. R. S. Webber, M. Bare, B. Cysyk, G. Krauss, and B. Gordon, "Brief bursts of pulse stimulation terminate afterdischarges caused by cortical stimulation," *Neurology*, vol. 53, no. 9, pp. 2073–2081, December 1999.
- [6] A. L. Velasco, M. Velasco, F. Velasco, D. Menes, F. Gordon, L. Rocha, M. Briones, and I. Mrquez, "Subacute and chronic electrical stimulation of the hippocampus on intractable temporal lobe seizures: Preliminary report," *Archives of Medical Research*, vol. 31, no. 3, pp. 316–328, May 2000.
- [7] N. Akamatsu, Y. Fueta, Y. Endo, K. Matsunaga, T. Uozumi, and S. Tsuji, "Decreased susceptibility to pentylenetetrazol-induced seizures after low-frequency transcranial magnetic stimulation in rats," *Neuroscience Letters*, vol. 310, no. 2, pp. 153–156, September 2001.
- [8] L. Iasemidis and J. Sackellares, "Chaos theory and epilepsy," pp. 118–126, 1996.
- [9] K. N. Fountas, J. R. Smith, A. M. Murro, Y. D. Park, P. D. Jenkins, and D. Greene, "Closed-loop stimulation implantable system for the management of focal, medically refractory epilepsy: Implantation technique and preliminary results," in *Annual Meeting of the American Epilepsy Society*, 2005.
- [10] J. M. Plitsky, R. Estellar, A. M. Murro, J. Smith, P. Ray, Y. D. Park, and M. J. Morrell, "Effects of electrical stimulation paradigm on seizure frequency in medically intractable partial seizure patients with a cranially implanted responsive cortical neurostimulator," in *Annual Meeting of the American Epilepsy Society*, 2005.
- [11] M. Derchansky, E. Shahar, R. Wennberg, M. Samoilova, S. Jahromi, P. Abdelmalik, L. Zhang, and P. Carlen, "Model of frequent, recurrent, and spontaneous seizures in the intact mouse hippocampus," *Hippocampus*, vol. 14, no. 8, pp. 935–947, April 2004.
- [12] M. L. V. Quyen, J. Martinerie, V. Navarro, P. Boon, M. D'Hav, C. Adam, B. Renault, D. Varela, and P. Baulac, "Anticipation of epileptic seizures from standard EEG recordings," *The Lancet*, vol. 357, no. 9251, pp. 183–188, January 2001.
- [13] B. Litt, R. Esteller, J. Echaz, M. D'Alessandro, R. Shor, T. Henry, P. Pennell, C. Epstein, R. Bakay, M. Dichter, and G. Vachtsevanos, "Epileptic seizures may begin hours in advance of clinical onset: A report of five patients," *Neuron*, vol. 30, no. 1, pp. 51–64, April 2001.
- [14] V. Navarro, J. Martinerie, M. L. V. Quyen, S. Clemenceau, C. Adam, M. Baulac, and F. Varela, "Seizure anticipation in human neocortical partial epilepsy," *Brain*, vol. 125, no. 3, pp. 640–655, March 2002.
- [15] K. K. Jerger, T. I. Netoff, J. T. Francis, T. Sauer, L. Pecora, S. L. Weinstein, and S. J. Schiff, "Comparison of methods for seizure detection," *Epilepsy as a Dynamic Diseases*, pp. 237–248, 2003.
- [16] A. W. L. Chiu, E. E. Kang, M. Derchansky, P. L. Carlen, and B. L. Bardakjian, "Online prediction of onsets of seizure-like events in hippocampal neural networks using wavelet artificial neural networks," *Annals of Biomedical Engineering*, vol. 34, no. 2, pp. 282–294, 2006.
- [17] F. Mormann, R. G. Andrzejak, C. E. Elger, and K. Lehnertz, "Seizure prediction: the long and winding road," *Brain*, vol. 130, no. 2, pp. 314–333, 2007.
- [18] H. Khosravani, P. L. Carlen, and J. L. P. Velazquez, "The control of seizure-like activity in the rat hippocampal slice," *Biophysical Journal*, vol. 84, no. 1, pp. 687–695, January 2003.
- [19] A. Chiu and B. Bardakjian, "Control of state transitions in an in silico model of epilepsy using small perturbations," *IEEE Transactions on Biomedical Engineering*, vol. 51, no. 10, pp. 1856–1859, October 2004.
- [20] S. S. Jahromi, K. Wentlandt, S. Piran, and P. L. Carlen, "Anticonvulsant actions of gap junctional blockers in an in vitro seizure model," *Journal of Neurophysiology*, vol. 88, no. 4, pp. 1893–1902, October 2002.
- [21] B. Lasztocki, K. Antal, L. Nyikos, Z. Emri, and J. Kardos, "High-frequency synaptic input contributes to seizure initiation in the low-Mg<sup>2+</sup> model of epilepsy," *European Journal of Neuroscience*, vol. 19, no. 5, pp. 1361–1372, March 2004.
- [22] K. Lehnertz and C. E. Elger, "Can epileptic seizures be predicted? Evidence from nonlinear time series analysis of brain electrical activity," *Physical review letters*, vol. 80, no. 22, pp. 5019–5022, 1998.
- [23] A. Chiu, S. Daniel, H. Khosravani, P. Carlen, and B. Bardakjian, "Prediction of seizure onset in an in-vitro hippocampal slice model of epilepsy using gaussian-based and wavelet-based artificial neural networks," *Annals of Biomedical Engineering*, vol. 33, no. 6, pp. 798–810, June 2005.
- [24] G. A. Worrell, L. Parish, S. D. Cranstoun, R. Jonas, G. Baltuch, and B. Litt, "High-frequency oscillations and seizure generation in neocortical epilepsy," *Brain*, vol. 127, no. 7, pp. 1496–1506, 2004.
- [25] V. I. Dzhalal and K. J. Staley, "Transition from interictal to ictal activity in limbic networks in vitro," *The Journal of Neuroscience*, vol. 23, no. 21, pp. 7873–7880, August 2003.
- [26] —, "Mechanisms of fast ripples in the hippocampus," *The Journal of Neuroscience*, vol. 24, no. 40, pp. 8896–8906, October 2004.
- [27] A. W. L. Chiu, S. S. Jahromi, H. Khosravani, P. L. Carlen, and B. L. Bardakjian, "The effects of high frequency oscillations in hippocampal electrical activities on the classification of epileptiform events using artificial neural networks," *Journal of Neural Engineering*, vol. 3, pp. 9–20, 2006.
- [28] S. Schiff, J. Milton, J. Heller, and S. Weinstein, "Wavelet transforms and surrogate data for electroencephalographic spike and seizure localization," *Optical Engineering*, vol. 33, no. 7, pp. 2162–2169, 1994.
- [29] M. Sun, M. L. Scheuer, and R. J. Scabassi, "Extraction and analysis of early ictal activity in subdural electroencephalogram," *Annals of Biomedical Engineering*, vol. 29, no. 10, pp. 878–886, November 2004.
- [30] O. Jensen and C. Tesche, "Frontal theta activity in humans increases with memory load in a working memory task," *European journal of Neuroscience*, vol. 15, pp. 1398–1399, 2002.
- [31] P. Goupillaud, A. Grossman, and J. Morlet, "Cycle-octave and related transforms in seismic signal analysis," *Geoexploration*, vol. 23, pp. 85–102, 1984.
- [32] S. Haykin, *Neural networks: A comprehensive foundation*, 2nd ed. Prentice-Hall, 1999.
- [33] J. P. Dreier and U. Heinemann, "Regional and time dependent variations of low Mg<sup>2+</sup> induced epileptiform activity in rat temporal cortex slices," *Experimental Brain Research*, vol. 87, no. 3, pp. 581–596, December 1991.
- [34] I. Osorio, M. G. Frei, and S. B. Wilkinson, "Real-time automated detection and quantitative analysis of seizures and short-term prediction of clinical onset," *Epilepsia*, vol. 39, no. 6, pp. 615–627, 1998.
- [35] I. Osorio, M. G. Frei, J. Giftakis, T. Peters, J. Ingram, M. Turnbull, M. Herzog, M. Rise, S. Schaffner, R. Wennberg, T. Walczak, M. Risinger, and C. Ajomone-Marsan, "Performance re-assessment of a real-time seizure detection algorithm on long ECoG series," *Epilepsia*, vol. 43, no. 12, pp. 1522–1535, December 2002.
- [36] Y. U. Khan and J. Gotman, "Wavelet based automatic seizure detection in intracerebral electroencephalogram," *Clinical Neurophysiology*, vol. 114, no. 5, pp. 898–908, May 2003.
- [37] H. Adeli, S. Ghosh-Dastidar, and N. Dadmehr, "A wavelet-chaos methodology for analysis of EEGs and EEG sub-bands to detect seizure and epilepsy," *IEEE Transactions on Biomedical Engineering*, vol. 54, no. 2, pp. 205–211, February 2007.
- [38] A. Subasi, A. Alkan, E. Koklukaya, and M. K. Kiyimik, "Wavelet neural network classification of EEG signals by using AR model with MLE preprocessing," *Neural Networks*, vol. 18, no. 7, pp. 985–997, September 2005.

- [39] A. Subasi, "Epileptic seizure detection using dynamic wavelet network," *Expert Systems with Applications*, vol. 29, no. 2, pp. 343–355, August 2005.
- [40] S. Kim, R. A. Normann, R. Harrison, and F. Solzbacher, "Preliminary study of the thermal impact of a microelectrode array implanted in the brain," in *IEEE Engineering in Medicine and Biology Conference*, 30 Aug–3 Sept 2006, pp. 2986–2989.
- [41] R. R. Harrison and C. Charles, "A low-power low-noise CMOS amplifier for neural recording applications," *IEEE Journal of Solid-State Circuits*, vol. 38, no. 6, pp. 958–965, June 2003.
- [42] T. Delbruck and C. A. Mead, "Adaptive photoreceptor with wide dynamic range," in *IEEE International Symposium on Circuits and Systems*, vol. 4, 30 May–2 June 1994, pp. 339–342.
- [43] P. Li, M. Chin, P. Gray, and R. Castello, "A ratio-independent algorithmic analog-to-digital conversion technique," *IEEE Journal of Solid-State Circuits*, vol. 19, no. 6, pp. 828–836, 1984.
- [44] W. R. Patterson, Y. K. Song, C. W. Bull, I. Ozden, A. P. Deangellis, C. Lay, J. L. McKay, A. V. Nurmikko, J. D. Donoghue, and B. W. Connors, "A microelectrode/microelectronic hybrid device for brain implantable neuroprosthesis applications," *IEEE Transactions on Biomedical Engineering*, vol. 51, no. 10, pp. 1845–1853, October 2004.
- [45] B. Eversmann, M. Jenkner, F. Hofmann, C. Paulus, R. Brederlow, B. Holzapfl, P. Fromherz, M. Merz, M. Brenner, M. Schreiter, R. Gabl, K. Plehnert, M. Steinhäuser, G. Eckstein, D. Schmitt-Landsiedel, and R. Thewes, "A  $128 \times 128$  CMOS biosensor array for extracellular recording of neural activity," *IEEE Journal of Solid-State Circuits*, vol. 38, no. 12, pp. 2306–2317, December 2003.
- [46] P. Mohseni and K. Najafi, "A fully integrated neural recording amplifier with DC input stabilization," *IEEE Transactions on Biomedical Engineering*, vol. 51, no. 5, pp. 832–837, May 2004.
- [47] M. Yin and M. Ghovanloo, "A low-noise preamplifier with adjustable gain and bandwidth for biopotential recording applications," in *Proceedings of the IEEE International Symposium on Circuits (ISCAS'07)*, May 2007, pp. 321–324.
- [48] J. Aziz, R. Genov, B. Bardakjian, M. Derchansky, and P. Carlen, "Brain-silicon interface for high-resolution in vitro neural recording," *IEEE Transactions on Biomedical Circuits and Systems*, April 2007.
- [49] M. Derchansky, D. Rokni, J. Rick, R. Wennberg, B. Bardakjian, L. Zhang, Y. Yarom, and P. Carlen, "Bidirectional multisite seizure propagation in the intact isolated hippocampus: The multifocality of the seizure "focus"," *Neurobiology of Disease*, vol. 23, no. 2, pp. 312–328, August 2006.
- [50] J. Aziz, R. Karakiewicz, R. Genov, B. Bardakjian, M. Derchansky, and P. Carlen, "Real-time seizure monitoring and spectral analysis microsystem," in *Proceedings of the IEEE International Symposium on Circuits (ISCAS'06)*, May 21–24 2006.
- [51] J. Aziz, R. Karakiewicz, R. Genov, A. Chiu, B. Bardakjian, M. Derchansky, and P. Carlen, "In vitro epileptic seizure prediction microsystem," in *Proceedings of the IEEE International Symposium on Circuits (ISCAS'07)*, May 21–24 2006, pp. 3115–3118.
- [52] R. R. Harrison, P. Watkins, R. Kier, R. Lovejoy, D. Black, R. Normann, and F. Solzbacher, "A low-power integrated circuit for a wireless 100-electrode neural recording system," in *IEEE International Conference Solid-State Circuits Digest of Technical Papers*. IEEE, 6–9 February 2006, pp. 2258–2267.
- [53] J. Aziz, R. Genov, M. Derchansky, B. Bardakjian, and P. Carlen, "256-channel neural recording microsystem with on-chip 3D electrodes," in *IEEE International Solid-State Circuits Conference Digest of Technical Papers*, 11–15 February 2007, pp. 160–161.
- [54] A. H. Kramer, "Array-based analog computation," *IEEE Micro*, vol. 16, no. 5, pp. 20–29, October 1996.
- [55] C. Rogers, J. Harris, J. Principe, and J. Sanchez, "An analog VLSI implementation of a multi-scale spike detection algorithm for extracellular neural recordings," pp. 213–216, March 2005.
- [56] R. Sarpeshkar, "Analog versus digital: Extrapolating from electronics to neurobiology," *Neural Computation*, vol. 10, pp. 1601–1638, 1998.
- [57] C. Neugebauer and A. Yariv, "A parallel analog CCD/CMOS neural network IC," in *Proceedings IEEE Int. Joint Conference on Neural Networks*, vol. 1, Seattle, WA, 1991, pp. 447–451.
- [58] R. Genov, G. Cauwenberghs, G. Mulliken, and F. Adil, "A 5.9 mW 6.5 GMACs CID/DRAM array processor," in *Proceedings IEEE European Solid-State Circuits Conference*, Sept. 2002, pp. 715–718.
- [59] R. Karakiewicz, R. Genov, and G. Cauwenberghs, "480-GMACS/mW resonant adiabatic mixed-signal processor array for charge-based pattern recognition," *IEEE Journal of Solid-State Circuits*, vol. 42, no. 11, November 2007.
- [60] R. Genov and G. Cauwenberghs, "Kerneltron: Support vector 'machine' in silicon," *IEEE Trans. Neural Networks*, vol. 14, no. 5, pp. 1424–1434, 2002.
- [61] S. Chakrabarty and G. Cauwenberghs, "Sub-microwatt analog VLSI trainable pattern classifier," *IEEE Journal of Solid-State Circuits*, vol. 42, no. 5, pp. 1169–1179, 2007.